Polyglycolic Acid–Polylactic Acid Scaffold Response to Different Progenitor Cell *In Vitro* Cultures: A Demonstrative and Comparative X-Ray Synchrotron Radiation Phase-Contrast Microtomography Study

Alessandra Giuliani, PhD,[1] Francesca Moroncini, PhD,[2] Serena Mazzoni, PhD,[1]
Marzia Laura Chiara Belicchi,[3] Chiara Villa,[3,4] Silvia Erratico, PhD,[5] Elena Colombo, PhD,[6]
Francesca Calcaterra,[6,7] Lucia Brambilla, MD,[8] Yvan Torrente, MD, PhD,[3,9]
Gianni Albertini,[2] and Silvia Della Bella, MD, PhD[6,7]

Spatiotemporal interactions play important roles in tissue development and function, especially in stem cell-seeded bioscaffolds. Cells interact with the surface of bioscaffold polymers and influence material-driven control of cell differentiation. *In vitro* cultures of different human progenitor cells, that is, endothelial colony-forming cells (ECFCs) from a healthy control and a patient with Kaposi sarcoma (an angioproliferative disease) and human CD133 + muscle-derived stem cells (MSH 133 + cells), were seeded onto polyglycolic acid–polylactic acid scaffolds. Three-dimensional (3D) images were obtained by X-ray phase-contrast microtomography (micro-CT) and processed with the Modified Bronnikov Algorithm. The method enabled high spatial resolution detection of the 3D structural organization of cells on the bioscaffold and evaluation of the way and rate at which cells modified the construct at different time points from seeding. The different cell types displayed significant differences in the proliferation rate. In conclusion, X-ray synchrotron radiation phase-contrast micro-CT analysis proved to be a useful and sensitive tool to investigate the spatiotemporal pattern of progenitor cell organization on a bioscaffold.

Introduction

Cᴇʟʟ ᴛʜᴇʀᴀᴘʏ ʀᴇsᴇᴀʀᴄʜ has long been trying to achieve repair of damaged tissue by creating *in vitro* tissue constructs for subsequent transplantation. A major factor hampering such endeavors is that the environment, where stem cells grow or are seeded, has critical, but poorly understood effects on their fate.[1–6] Choosing the internal structure of a scaffold is a major decision involving a variety of parameters such as phase composition, porosity, pore size, and interconnectivity. These factors affect the transportation of nutrients that enable cell growth and proliferation and make the scaffold a suitable template for tissue growth and, eventually, repair.[7–11] A number of biomaterials ranging

from naturally derived materials (e.g., silk-based materials, collagen, and alginate)[12,13] to cellular tissue matrices (e.g., bladder submucosa and small intestinal submucosa)[14–17] and synthetic polymers like polyglycolic acid (PGA), polylactic acid (PLLA), and poly(lactic-co-glycolic acid) (PLGA)[11,18–20] have been used to obtain engineered tissue. *In vitro*-engineered muscle and endothelial tissue seeded on synthetic polymers have some key advantages, including the facts that such scaffolds degrade by nonenzymatic hydrolysis and that the degradation products of PGA, PLLA, and PLGA are nontoxic, naturally metabolized, and are eventually eliminated from the body as carbon dioxide and water.[19]

The kinetics of early stage *in vitro* tissue formation is still unclear. Common laboratory protocols typically subject

[1]Dipartimento di Scienze Cliniche Specialistiche e Odontostomatologiche, Università Politecnica delle Marche, Ancona, Italy.
[2]Dipartimento di Scienze e Ingegneria della Materia dell'Ambiente ed Urbanistica, Università Politecnica delle Marche, Ancona, Italy.
[3]Stem Cell Laboratory, Department of Pathophysiology and Transplantation, Fondazione IRCCS Ca' Granda Ospedale Maggiore Policlinico, Centro Dino Ferrari, Università degli Studi di Milano, Milano, Italy.
[4]Diabetes Research Institute, University of Miami, Coral Gables, Florida.
[5]Ystem Srl, Milano, Italy.
[6]Lab of Clinical and Experimental Immunology, Humanitas Clinical and Research Center, Rozzano (MI), Italy.
[7]Department of Medical Biotechnologies and Translational Medicine, University of Milan, Milan, Italy.
[8]Fondazione IRCSS Ca' Granda Ospedale Maggiore Policlinico U.O. Dermatologia, University of Milan, Milan, Italy.
[9]Centro Interdipartimentale di Ricerca sulle Cellule Staminali (UNISTEM), Milano, Italy.

tissue-engineered specimens only to histological analysis and electron microscopy examination, to characterize their constituent elements in two dimensional (2D).[21,22] In this field, three-dimensional (3D) visualization techniques can help gain a greater understanding.

X-ray computed microtomography (micro-CT), one of the most common 3D imaging techniques, has been applied to the qualitative and quantitative evaluation of tissue growth under different conditions, including engineered bone,[3,7,8,23] tendon,[24] and heart.[25] However, data regarding the application of X-ray-based techniques to complex constructs such as those involved in muscle and vessel tissue engineering, including stem cell visualization, are still limited. Recently, X-ray micro-CT analysis was applied to study stem cells *ex vivo*[26] and *in vivo*,[27] providing high-definition and high-resolution 3D images of human cells labeled with magnetic nanoparticles and transplanted by intra-arterial infusion. Whereas soft tissue investigation by attenuation-based X-ray imaging methods without contrast agents is hampered by poor contrast, phase-sensitive techniques afford enhanced contrast where absorption is insufficient, for instance, to detect the extracellular matrix (ECM) and vessel structures. Phase-contrast X-ray imaging (PCI) is sensitive to light elements such as hydrogen, carbon, nitrogen, and oxygen, which are commonly found in soft tissue. The phase-contrast arises because both the amplitude and phase are modified as the X-ray beam propagates through tissue. Since the probability for X-ray phase shift can be 1000 times greater than for X-ray attenuation in the keV energy range, phase-contrast imaging affords visualization of soft tissues with identical or similar attenuation characteristics, which would not be detected using conventional attenuation-based X-ray imaging methods. Moreover, because the refractive index-based image contrast decreases less rapidly with increasing X-ray energy compared with attenuation-based contrast, phase-contrast imaging enables reduction of the radiation dose delivered.[28] Recently, Albertini *et al.*[11] obtained 3D PCI micro-CT images of *in vitro* ECM organization in bone marrow-derived human and murine mesenchymal stem cells after induction of myogenic differentiation on PGA/PLLA fiber scaffolds. Unfortunately, the simpler phase-contrast imaging settings do not automatically provide quantitative phase data suitable for tomographic reconstruction, meaning that phase-retrieval algorithms are often required. The reconstruction algorithm suggested by Bronnikov[29,30] provides an alternative to the conventional approach by making phase retrieval superfluous. His one-step approach is also extremely simple and keeps the radiation dose to a minimum, which is very important for biological specimens.

In this work, we demonstrate that PCI micro-CT combined with the Modified Bronnikov Algorithm (MBA) as described by Groso *et al.*[31] is suitable to study the early stages of *in vitro* tissue formation using human CD133+ muscle-derived stem cells (MSH 133+ cells) and human endothelial colony-forming cells (ECFCs) cultured on the PGA/PLLA fiber scaffolds used by our group in a previous article.[11]

Materials and Methods

Scaffold material

PGA/PLLA fibers (Fig. 1A) are biocompatible and bioresorbable. The scaffolds used in this study were made of biofelt (produced by Concordia Fibers) containing equal (50–50) proportions of nonwoven PGA and PLLA fibers. The biofelt had a thickness of 0.5 mm and a density of 50 mg/cc.; the average and nominal fiber diameter was 18 μm. The pore size was in the 50–200 μm range (Fig. 1B). Due to the highly porous structure of the felt (>97%), the pores are interconnected. The characteristics of these scaffolds were identical to those of the biomaterials used in a previous work by our group.[11]

Isolation and culture of ECFCs

ECFCs were isolated and cultured from peripheral blood mononuclear cells (PBMCs) according to previously described methods.[32,33] Briefly, PBMCs were obtained by Ficoll density gradient centrifugation (Cedarlane) from 30 mL of fresh venous blood collected from a healthy donor (HD) and from a patient with stage 4B classic Kaposi sarcoma (KS) based on the criteria proposed by Brambilla *et al.*[34,35] The
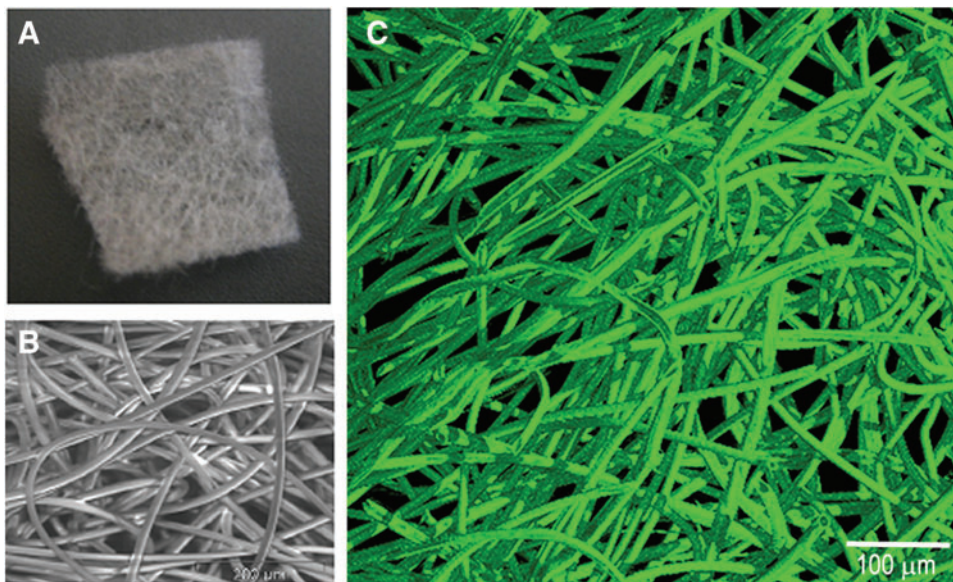

FIG. 1. Pure fiber polyglycolic acid–polylactic acid (PGA/PLLA) scaffold. Light **(A)** and scanning electron microscopy **(B)** images[11]; **(C)** Three-dimensional (3D) micro-CT reconstruction of a PGA/PLLA scaffold cultured without cells. Color images available online at www.liebertpub.com/tec

patient gave his informed consent to participate in the study. PBMCs were resuspended in the EGM-2 medium (Cambrex Bio Science) and seeded at a density of 5×10^6 cells/well onto 24-well tissue culture plates precoated with human fibronectin ($1 \mu g/cm^2$; Sigma-Aldrich). After 1 day of culture, nonadherent cells and debris were aspirated and adherent cells were washed with the EGM-2 medium. The medium was then added to each well and changed every 2 days until the first passage. An inverted microscope was used to determine the initial formation of visible colonies. These were identified as well-defined monolayers of cobblestone-like cells. ECFC colonies were detached from culture plates by treatment with trypsin (0.25%) (Euroclone), resuspended in the EGM-2 medium, and plated onto 10-cm^2 tissue culture plates precoated with type I rat-tail collagen (BD Biosciences). Subconfluent cells were further subpassaged and expanded. At each passage, viable cell counts were obtained using a hemocytometer and trypan blue exclusion. Passage 4 ECFCs were seeded on the PGA/PLLA scaffolds, which had been plated in 24-well plates precoated with agarose 2%. Based on preliminary experiments, 0.75×10^6 cells/well were seeded and cultured in the EGM-2 medium at 37°C in a CO_2 (5%) incubator. After 6 (Fig. 2A) or 12 (Fig. 2B) days in culture, one of the samples was washed in phosphate-buffered saline (PBS) stained with hematoxylin–eosin (H&E) and examined by light microscopy. Parallel samples were washed, fixed in 4% paraformaldehyde (PFA) for 30 min, and kept in ethanol 70% for micro-CT imaging.

Isolation and culture of muscle CD133+ stem cells (MSH 133+)

Primary human muscle cells were obtained from biceps brachial muscle biopsies by enzymatic dissociation.
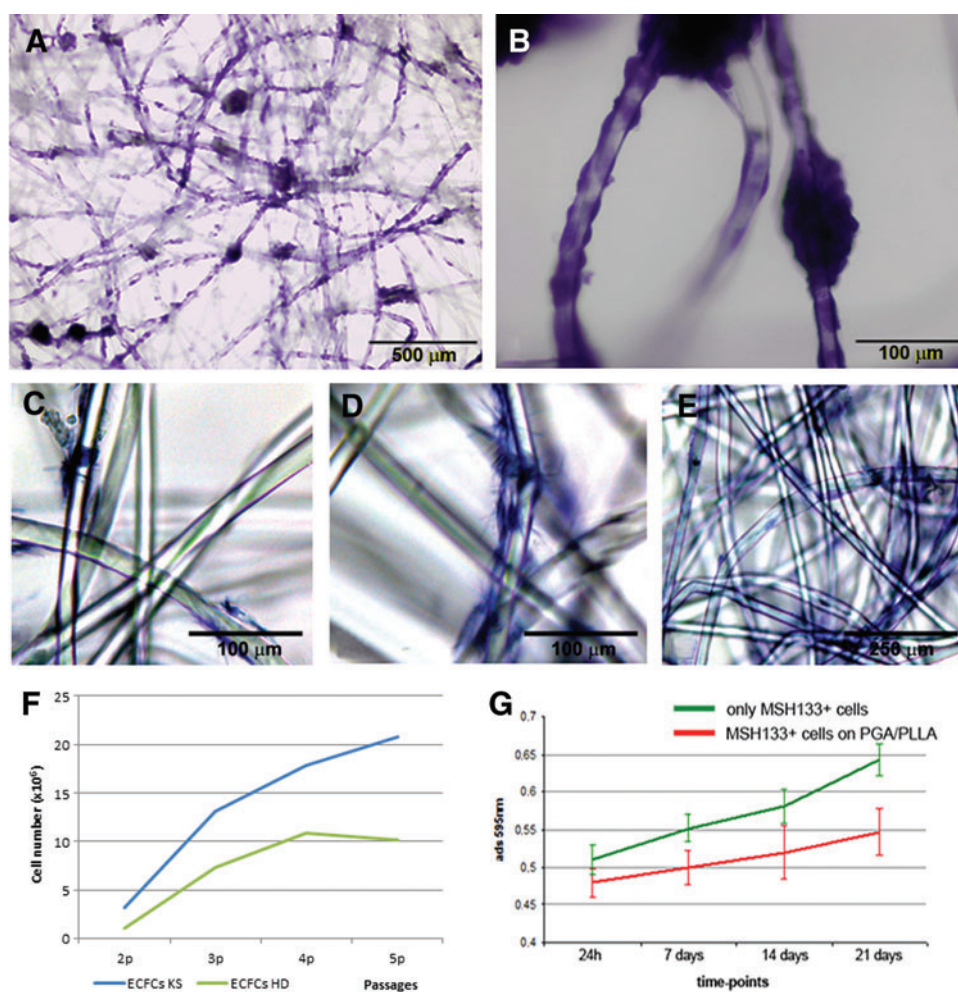

FIG. 2. **(A, B)** PGA/PLLA scaffolds seeded with human endothelial colony-forming cells (ECFCs) cultured for 6 days in the proliferation medium at $4 \times$ magnification **(A)** and $20 \times$ magnification **(B)**. ECFCs clearly adhere to the scaffold and are arranged along the PGA/PLLA fibers. **(C–E)** PGA/PLLA scaffolds cultured with human muscle-derived CD133+ (MSH 133+) cells grown for 7 **(C)**, 14 **(D)**, and 21 **(E)** days in the proliferation medium. MSH 133+ cells clearly adhere to the scaffold and are arranged along the PGA/PLLA fibers. **(F)** Growth curves of ECFCs from the patient with Kaposi sarcoma (KS ECFCs) and from the healthy donor (HD ECFCs) showing a greater proliferation rate of KS ECFCs. The cell yield counted at the end of each passage is reported. **(G)** MTT assay. The curves show a different MSH 133+ cell proliferation kinetics on PGA/PLLA scaffolds and control plates. Three wells were analyzed for each culture condition; measurements were performed 24 h from seeding and at 7, 14, and 21 days of culture. Color images available online at www.liebertpub.com/tec

Mononuclear cells from muscle were then processed through the MACS magnetic separation column (Miltenyi Biotec). The purity of selected MSH 133+ cells was determined for each isolation experiment. Cells were then plated in a proliferation medium consisting of DMEM/F-12 (1:1), 10% FBS, including glucose (0.6%), glutamine (2 mM), SCF (100 ng/ mL; TEBU-BIO), VEGF (50 ng/mL; TEBU-BIO), and LIF (20 ng/mL; R&D Systems). Cell viability was assayed using 7-amino-actinomycin D (7-AAD). For five-color flow cytometric analysis, at least 10×10^4 up to 20×10^4 dissociated muscle cells were incubated with the following monoclonal antibodies: anti-CD45 fluorescein isothiocyanate (FITC), anti-CD34 allophycocyanin (APC), anti- CD31 FITC, anti-CD184 (CXCR4/fusin), and PE-Cy5 (all from BD Bioscences-Pharmingen), and anti-CD133 phycoerythrin (PE; Miltenyi Biotec). For each antibody, an appropriate isotype-matched mouse immunoglobulin was used as a control. After incubation at 4°C for 20 min, cell suspensions were washed in PBS containing 1% heat-inactivated fetal calf serum and 0.1% sodium azide. A light-scatter gate was added to exclude nonviable cells from the analysis. Flow cytometric analysis was performed on a Facs Cytomics FC500 apparatus with CXP 2.1 software (Beckman Coulter).

After a short *ex vivo* proliferation period (about 10 days), MSH 133+ cells were seeded on the PGA/PLLA scaffold; 2×10^5 cells were resuspended in 200 μL of proliferation medium and seeded by gravity on the scaffold precoated with laminin 10 μg/mL (Sigma-Aldrich). The cell-seeded scaffold was plated in a 24-well plate precoated with agarose 2% and incubated in fully humidified atmosphere of 5% CO_2, 95% air at 37°C. A fresh medium was added after 2 h.

After 7 (Fig. 2C), 14 (Fig. 2D) or 21 (Fig. 2E) days in culture, one sample per group was washed in PBS, stained with H&E, and examined by light microscopy. The proliferation capacity of MSH 133+ cells was evaluated by seeding the scaffold with the cell suspension (density, 1×10^5 cells/mL). Cell proliferation and scaffold cytotoxicity were analyzed with the 3-(4,5-dimethylthiazol-2-yl)-2,5-diphenyl tetrazolium bromide (MTT) assay (Roche) (Fig. 2G). Cell-seeded scaffolds were removed after the desired incubation at 37°C. As a negative control, cells were seeded at the same density (1×10^5 cells/mL) in laminin-coated tissue culture plates for the same time periods as the experimental samples (7, 14, or 21 days). The MTT assay was performed on alternate days. On test days, the medium was removed from both experimental and control wells, which were washed with cold PBS, pH 7.4; the MTT solution at a concentration of 0.5 mg/mL (0.5 mL) was added to all wells, followed by incubation for 4–5 h at 37°C in a humid environment with 5% CO_2. Subsequently, MTT was gently removed and 1.5 mL dimethyl sulfoxide (DMSO) was added. Plates were again incubated for 15–20 min at 37°C with 5% CO_2. After incubation, the color was measured spectrophotometrically at 570 nm to estimate relative cell viability. The scaffolds were analyzed in triplicate to minimize variation. Parallel samples were washed in PBS, fixed in 4% PFA for 30 min, and kept in 70% ethanol for micro-CT analysis.

X-ray micro-CT

X-ray tomographic microscopy experiments were performed at the TOMCAT beamline of the Swiss Light Source (Paul Scherrer Institut).[36] Six groups of samples, each consisting of three identical cell-seeded PGA/PLLA scaffolds, and a group of three control samples were examined: KS ECFCs cultured at 6 days; KS ECFCs cultured at 12 days; HD ECFCs cultured at 6 days; HD ECFCs cultured at 12 days; MSH 133+ cultured at 14 days; and MSH 133+ cultured at 21 days. Control samples consisted of scaffolds cultured in standard wells without cells. Samples were examined at $10 \times$ optical magnification with no binning, isometric voxel with edge size of 740 nm (spatial resolution is typically approximated at two to three times the pixel size); exposure time 240 ms/projection; and energy 19 keV, which was preliminarily found to provide acceptable imaging of both the polymeric scaffolds and cells, whereas at the same time minimizing the thermal effect (reducing the absorption signal with energy increase). A sample-detector distance of 57 mm enabled phase contrast through edge enhancement. The CCD camera was a 2048×2048 pixel chip (7.4×7.4 μm^2 pitch) equipped with four GB internal RAM memory (camRAM). Images were acquired up to 14.7 frames/s at full frame.

The approach used in this work, that is, phase contrast through edge enhancement, differs from conventional X-ray tomography because the resulting images are not based solely on attenuation contrast. The effect of an X-ray beam going through the sample is described by the refractive index, $n = 1 - \delta + \iota\beta$, where δ is the refractive index decrement (typically around 10^{-6}) and β is the attenuation index. The fact that δ is much larger than the imaginary part β demonstrates that the phase approach provides greater sensitivity than the absorption approach. δ is actually proportional to the mean electron density, which in turn is nearly proportional to the mass density.

The MBA was used during dataset reconstruction.[31] Typically, the methods used for quantitative volumetric reconstructions of the refractive index in phase-contrast tomography are based on a two-step approach: first, the phase projections are determined in the form of radon projections (phase retrieval) and then the object function, that is, the refractive index decrement δ, is reconstructed by applying a conventional filtered back projection (FBP) or similar algorithm. As an alternative, Bronnikov suggested an algorithm that eliminates the intermediate phase retrieval step and provides direct reconstruction of the refractive index of the object. At TOMCAT, the MBA is successfully implemented by applying a filter representing the distribution of δ as described by Groso *et al.*[31] As shown by De Witte,[37] FBP slices are usually very sharp, but the reconstructions suffer from severe phase artifacts, which make structures that should be fairly homogeneous appear to consist of a very dense edge and an inner region with very low density that is hardly distinguishable from background noise. This would have adversely affected our experiment by affecting the quantitative analysis; however, in the MBA slices, the phase artifacts normally disappear almost completely, even though slices become more blurry and lose some detail. This was considered to be acceptable, because the monochromatic beam delivered by the synchrotron in our experimental setup, compared with De Witte's, entail sharply outlined phase shifts in the original projections, limiting image blurring.

The different phases shown in the histogram, where the different gray values (proportional δ) are reconstructed, were

colored using a 3D display software to make them easier to distinguish. Volume rendering is a 3D visualization method by which data volumes are rendered directly, without the need for decomposition into geometric primitives. A Quad-Core Processor 2.01 GHz PC with 8 GB RAM and the commercial software VG Studio MAX 1.2 (Volume Graphics) were used to generate 3D images and visualize the phase distribution in 3D. Optimal image quality settings were obtained using the Scatter HQ algorithm with an oversampling factor of 5.0 and activated color rendering. X-ray contrast differences within samples translate into different peaks in the gray-level scale, corresponding to the different phases. The volume of each phase is obtained by multiplying the volume of a voxel ($\sim 0.4\,\mu m^3$) by the number of voxels underlying the peak associated with the relevant phase. The Mixture Modeling algorithm (NIH ImageJ Plugin) was implemented to threshold the histograms. Thresholded slices were used to automatically separate the new cell-derived phase from the scaffold phase. The threshold of the newly formed phase was ~ 168 for scaffolds cultured with ECFCs and ~ 177 for those cultured with MSH 133+ cells. The difference was consistently found in all samples and may be due to the different origin of the cells, and consequently, to the different contrast with the PGA/PLLA scaffold.

Results

Cells

Adhesion of ECFCs to PGA/PLLA fibers was documented by light microscopy after H&E staining (Fig. 2A, B), although the 3D nature of the scaffold did not allow reliable quantification of adherent cells.

Adhesion of MSH 133+ cells to the scaffold was also clearly evident (Fig. 2C–E) and was subject to the same quantification limitations. MSH 133+ cell proliferation was further assessed by the MTT assay, to investigate PGA/PLLA cytotoxicity. The scaffold proved suitable for growth of MSH 133+ cells, which survived and proliferated although with a different kinetics compared with control cells cultured on standard wells; in particular, in the first week, absorbance was high in the 2D system (controls), but low on the 3D scaffold (Fig. 2G). Therefore, whereas control MSH 133+ cells proliferated over the first 7 days, those growing onto the scaffold took longer to adhere and then to begin proliferating. The MTT assay excluded PGA/PLLA scaffold-induced cytotoxic effects and highlighted the need for delaying micro-CT observation of MSH 133+ cell-seeded scaffolds until 14–21 days compared with ECFC-seeded scaffolds.

Another parameter tested in the study was the preservation of the differentiation capacity of MSH 133+ cells. In the experimental condition favoring muscle differentiation, that is, low serum concentration, the MSH 133+ cells grew along PGA/PLLA fibers; they expressed desmin, but did not exhibit visible myotubes. Such a delayed differentiation process may be connected with the longer time required for these cells to adhere to the scaffold.

Micro-CT

The 3D micro-CT analysis easily distinguished PGA/PLLA structures from the newly formed phase. Cell–scaffold interactions modified the bioresorbable PGA/PLLA structure, yielding images where two different phases had different δ values. To enhance visualization, the different phases were colored using the 3D display software: green for unchanged PGA/PLLA fibers and magenta for the contrast induced by cells, cell clusters, and portions of fibrillary matrix produced by cells growing on the bioscaffold. The magenta phase was easily recognizable in all scaffolds (ECFCs: Fig. 3a–d; MSH 133+ cells: Fig. 3e–f), but the one cultured without cells (Fig. 1C). The magenta phase mainly covers the fibers, preferentially choosing specific fibers (Fig. 3a–f), possibly the PGA ones. Recent studies have shown that the hydrophobic surface of PLLA scaffolds results in decreased cell adhesion compared with PGA constructs.[38]

The major finding was that ECFCs (whether KS or HD) produced a highly significantly ($p < 0.001$) greater amount of newly formed structures than MSH 133+ cells. This is clearly depicted in Figure 4, plotting the intensity counts versus the decrement of the refractive index δ. These profiles (including the inset) confirmed that the contrast produced by MSH 133+ cells over 14–21 days of culture was negligible compared with the signal produced by ECFCs over 6–12 days in the same conditions in a comparable PGA/PLLA volume, corresponding to the integrated area of the peak in Figure 4 (left).

The results of quantitative data analysis as a function of time from seeding are reported in Table 1, where scaffolds seeded with ECFCs are compared with those seeded with MSH 133+ cells. Data are shown as CV/FV, that is, the volume ratio of the cell-derived structure (CV) to the PGA-PLLA fiber volume (FV). The sample surface/sample volume (SS/SV) ratio and the fiber surface/fiber volume (FS/FV) ratio are also reported, to provide reliable quantitative information on cell proliferation potential. The mean fiber number (mm^{-1}) and the mean fiber distance (μm) were not included in the quantitative analysis because these parameters could be affected by postculture handling and fixation in the sample holder since PGA/PLLA scaffolds are not rigid. The need for postculture handling is also why we opted for normalizing the cell volume to fiber volume, not total volume. Another reason for this decision was the remodeling/resorption undergone by the scaffold over time, due to interaction with the cells. All the quantitative data are shown as mean ± standard deviation (SD).

Different rates of proliferation involved different amounts of tissue produced by ECFCs and MSH 133+ cells. Cell proliferation rates were more than 10-fold greater in HD ECFCs versus MSH 133+ cells, confirming the limited ability of MSH 133+ cells to adhere to and proliferate on this scaffold. It has been reported that MSH 133+ cells achieved 29.95 and 25.05 population doubling levels (PDLs) for CD133+ to CD34+ and CD133+ to CD34− cells, respectively, in 50 days of culture in standard proliferation conditions on noncoated polystyrene plates; since the value reported for human myoblasts is 17.00 PDLs, MSH 133+ cell proliferation rates are high.[39,40]

Interestingly, comparison of the proliferation rate of KS ECFCs and HD ECFCs at 6 and 12 days showed more than double CV/FV ratios in the former culture, possibly depending on the angioproliferative nature of KS.[41] To gain further insights into the proliferation rates of KS and HD
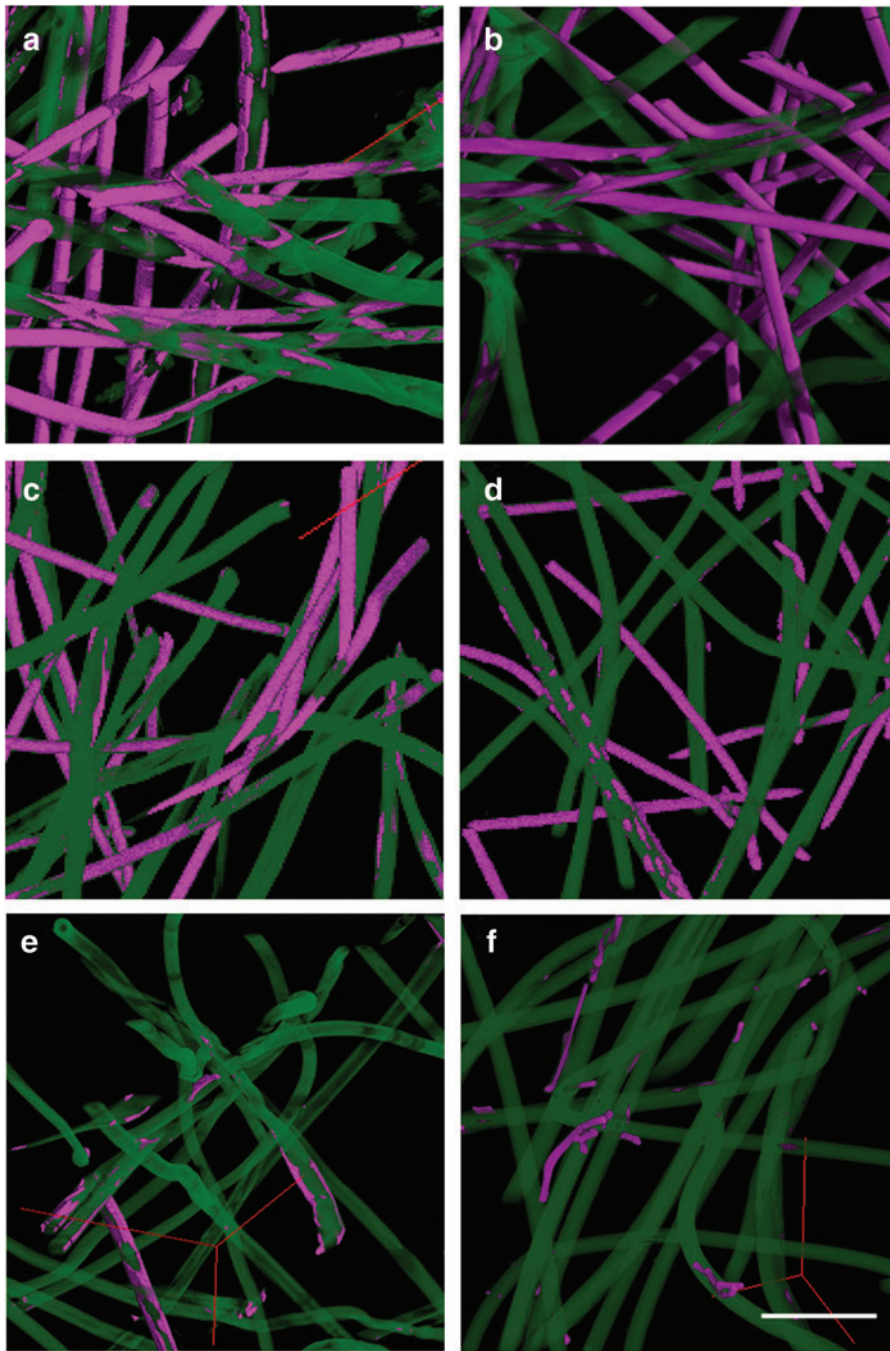
FIG. 3. X-Ray Synchrotron Radiation Phase-Contrast Microtomography 3D images of sample subvolumes. The interaction between cells and the polyglycolic acid–polylactic acid (PGA/PLLA) scaffold produces images with two different phases, corresponding to different δ (refractive index decrement) values. PGA/PLLA fibers are colored in green, whereas the contrast produced by cells, cell clusters, and ECM layers are colored in magenta. The images show that the scaffold cultured with ECFCs, whether from the Kaposi sarcoma patient [**(a)** 6 days of culture; **(b)** 12 days of culture or the healthy donor **(c)** 6 days of culture; **(d)** 12 days of culture] produced a significantly greater amount of newly formed structure than MSH 133+ cells [**(e)** 14 days of culture; **(f)** 21 days of culture]. Bar: 100 μm. Color images available online at www.liebertpub.com/tec

ECFCs, cell counts at the end of each passage were also performed in parallel cultures plated on collagen. The cell yield was greater in KS ECFCs, again suggesting that the higher CV/FV ratios found by micro-CT may reflect the higher proliferation potential of these cells.

An additional finding was that the CV/FV ratio rose in ECFCs and MSH 133+ cells with time from seeding, although the difference was significant ($p = 0.05$) only in HD ECFCs.

The SS/SV and FS/FV ratios were calculated to assess the rate of cell adhesion to the scaffold, which is directly related to the rate of PGA/PLLA scaffold resorption. In ECFC cultures, SS/SV was stable independently of culture time and cell donor, whereas in MSH 133+ cells it was highly signif-

icantly lower ($p < 0.001$). This is consistent with the mean fiber thickness measured in the different cultures at different times, that is, ~ 4–$5\,\mu$m in ECFCs and $\sim 10\,\mu$m in MSH 133+ cells. This evidence, which was further confirmed by the higher FS/FV values found in ECFC versus MSH 133+ cell cultures, supports the notion of a stronger interaction of ECFCs with the PGA/PLLA scaffold. Indeed, aside from the physiological reduction of mean fiber thickness due to spontaneous hydrolysis during culture, such stronger adhesion of ECFCs compared with MSH 133+ cells seems to accelerate scaffold resorption even after shorter times. In fact, although degradation of bioresorbable polymers occurs mainly by simple hydrolysis, cases of at least partial enzyme-mediated PGA and PLLA degradation have also been reported.[42,43]

FIG. 4. Profile of the intensity counts versus refractive index decrement δ. The integrated areas of the peaks on the left side (X-value ~140–145) correspond to the PGA/PLLA volume in scaffolds cultured with ECFC and MSH 133+ cells: their values are comparable. The peaks on the right side (X-value ~185–190) are the contrast produced after culture: the contrast generated by MSH 133+ cells over 14–21 days of culture is negligible compared with that produced by ECFCs over 6–12 days on the same PGA-PLLA scaffold. Color images available online at www.liebert pub.com/tec
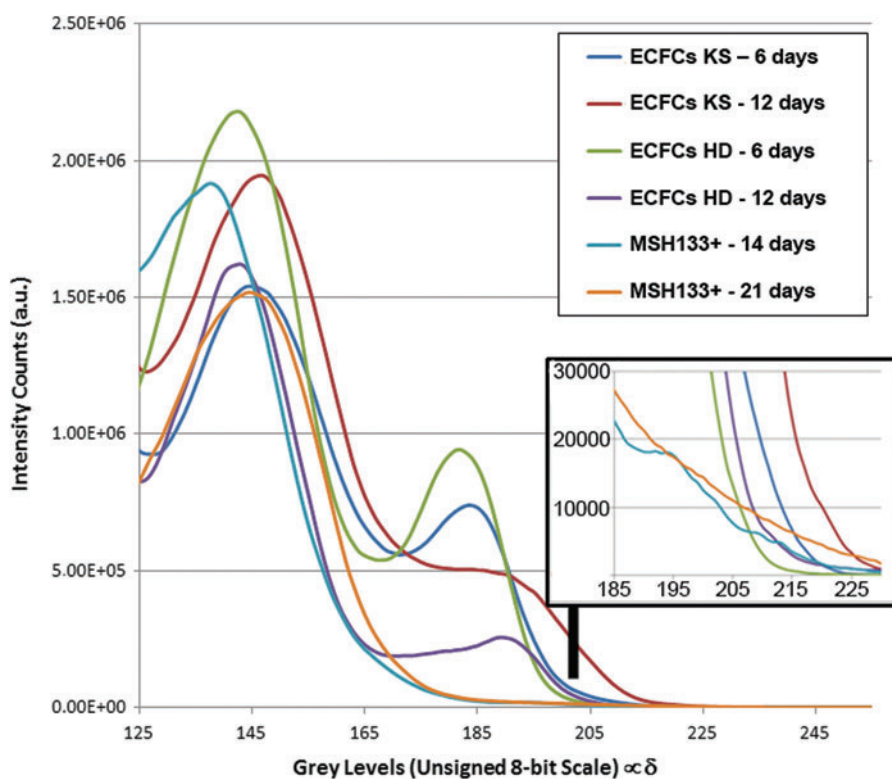
Discussion

A critical goal in tissue engineering is to obtain scaffolds with tailored physical, mechanical, and biological properties to act as substrates for cell growth and proliferation and as supports for new tissue formation.[44] Scaffolds capable of mimicking the ECM architecture and biological functions are promising candidates, because they are required to provide mechanical support, carry inductive molecules or cells, and supply signals to control the structure and function of newly formed tissue. Cell adhesion to the substrate is necessary for good polymer–cell interactions. Even though a scaffold is not required to have ECM-like characteristics for cell adhesion to occur, physicochemical similarity is nonetheless desired when aiming at promoting cell differentiation or a more effective interaction of a polymer at the implantation site.[45–48] Importantly, cell adhesion must occur before cell spreading and division and synthesis of a new ECM.[49,50]

This article presents a demonstrative application of X-ray phase-contrast micro-CT to the characterization of early-stage *in vitro* tissue formation on PGA/PLLA fiber scaffolds seeded with MSH 133+ stem cells and human ECFCs from a KS patient and a HD. The method disclosed thin-layered/spotted tissue deposits onto selected PGA/PLLA fibers with high resolution and in 3D. KS ECFCs displayed more than double CV/FV ratios than HD ECFCs. The proliferation rate of HD ECFCs on the scaffold was more than 10-fold greater versus MSH 133+ cells. The poor proliferation of MSH 133+ cells on PGA/PLLA may be due to the fact that these cells take longer to attach to the matrix and then start (slowly) proliferating, as shown by the MTT assay.

These same observations, conducted by conventional microscopy, failed to provide reliable quantitative information on cell proliferation potential on the scaffold at different culture times.

Micro-CT studies looking at scaffold changes over time, like ours, are still challenging and need proper boundary conditions. More powerful detection systems are needed to investigate larger scaffolds preserving high spatial resolutions. This will provide reliable quantitative data when scaffolds undergoing remodeling (like cell adhesion, proliferation, and differentiation on a bioresorbable scaffold) require segmentation.

TABLE 1. QUANTITATIVE ANALYSIS OF THREE-DIMENSIONAL DATA AFTER THE *IN VITRO* TESTS

	KS ECFCs		HD ECFCs		MSH 133+	
	6 days	*12 days*	*6 days*	*12 days*	*14 days*	*21 days*
CV/FV [%]	53.4±6.5	57.3±14.7	16.2±2.6	20.9±1.3	1.2±0.9	1.9±0.7
SS/SV [mm^{-1}]	246±4	252±4	245±5	249±6	224±13	217±6
FS/FV [mm^{-1}]	476±33	473±20	413±27	365±14	230±15	227±11

The whole samples are considered.
CV/FV, volume ratio of the cell-derived structure (CV) volume to the PGA-PLLA fiber volume (FV); SS/SV, sample surface to sample volume ratio; FS/FV, fiber surface to fiber volume ratio; ECFCs, endothelial colony-forming cells; KS, Kaposi sarcoma; HD, healthy donor.

Notably, absorption-based micro-CT is not recommended for analysis of soft tissues in such samples, due to low X-ray absorption by cells and scaffolds.[3,51] On the other hand, the use of synchrotron X-rays has several advantages over laboratory or industrial X-ray sources, including a high photon flux, which provides high spatial resolution measurements; a tunable X-ray source, allowing measurement at different energy levels; use of monochromatic X-ray radiation, which eliminates beam hardening effects; and parallel beam acquisition, which enables use of exact tomographic reconstruction algorithms.

Our experiments were conducted with a phase-contrast setup and subsequent application of the MBA to reconstruct the virtual volumes. The MBA successfully reconstructs the distribution of δ by applying a filter on samples characterized by low X-ray attenuation coefficients.

In conclusion, this article describes and demonstrates the feasibility of synchrotron micro-CT analysis to study cell proliferation on PGA/PLLA bioscaffolds. In general, it showed that noninvasive and quantitative X-ray micro-CT may be an important tool for exciting new applications in tissue engineering research.

Acknowledgments

Disclosure Statement

No competing financial interests exist.

References

1. Gomes, M.E., Bossano, C.M., Johnston, C.M., Reis, R.L., and Mikos, A.G. In vitro localization of bone growth factors in constructs of biodegradable scaffolds seeded with marrow stromal cells and cultured in a flow perfusion bioreactor. Tissue Eng **12,** 177, 2006.

2. Rada, T, Reis, R.L., and Gomes, M.E. Adipose tissue-derived stem cells and their application in bone and cartilage tissue engineering. Tissue Eng Part B Rev **15,** 113, 2009.

3. Giuliani, A., Fiori, F., Manescu, A., Komlev, V.S., Renghini, C., and Rustichelli, F. Synchrotron Radiation and Nanotechnology for Stem Cell Research. In: Gholamrezanezhad, A., ed. Stem Cells in Clinic and Research. InTech, Rijeka, Croatia, 2011, pp. 683–708.

4. Giuliani, A., Manescu, A., Langer, M., Rustichelli, F., Desiderio, V., Paino, F., De Rosa, A., Laino, L., d'Aquino, R., Tirino, V. et al. Three years after transplants in human mandibles, histological and in-line HT revealed that stem cells regenerated a compact rather than a spongy bone: biological and clinical implication. Stem Cells Trans Med **2,** 316, 2013.

5. Moon, S.U., Kim, J., Bokara, K.K., Kim, J.Y., Khang, D., Webster, T.J., and Lee, J.E. Carbon nanotubes impregnated with subventricular zone neural progenitor cells promotes recovery from stroke. Int J Nanomed **7,** 2751, 2012.

6. Belicchi, M., Cancedda, R., Cedola, A., Fiori, F., Gavina, M., Giuliani, A., Komlev, V.S., Lagomarsino, S., Mastrogiacomo, M., Renghini, C., Rustichelli, F., Syková, E., and Torrente, Y. Some applications of nanotechnologies in stem cells research. Mater Sci Eng B **3,** 139, 2009.

7. Cancedda, R., Cedola, A., Giuliani, A., Komlev, V., Lagomarsino, S., Mastrogiacomo, M., Peyrin, F., and Rustichelli, F. Bulk and interface investigations of scaffolds and tissue-engineered bones by X-ray microtomography and X-ray microdiffraction. Biomaterials **28,** 2505, 2007.

8. Renghini, C., Giuliani, A., Mazzoni, S., Brun, F., Larsson, E., Baino, F., and Vitale-Brovarone, C. Microstructural characterization and in vitro bioactivity of porous glass-ceramic scaffolds for bone regeneration by synchrotron radiation X-ray microtomography. J Eur Ceramic Soc **33,** 1553, 2013.

9. Pariente, J.L., Kim, B.S., and Atala, A. In vitro biocompatibility assessment of naturally derived and synthetic biomaterials using normal human urothelial cells. J Biomed Mater Res **55,** 33, 2001.

10. Cancedda, R., Dozin, B., Giannoni, P., et al. Tissue engineering and cell therapy of cartilage and bone. Matrix Biol **22,** 81, 2003.

11. Albertini, G., Giuliani, A., Komlev, V., Moroncini, F., Pugnaloni, A., Pennesi, G., Belicchi, M., Rubini, C., Rustichelli, F., Tasso, R., and Torrente, Y. Organization of extracellular matrix fibers within polyglycolic acid-polylactic acid scaffolds analyzed using X-ray synchrotron-radiation phase-contrast micro computed tomography. Tissue Eng Part C Methods **15,** 403, 2009.

12. Correia, C., Bhumiratana, S., Yan, L.P., Oliveira, A.L., Gimble, J.M., Rockwood, D., Kaplan, D.L., Sousa, R.A., Reis, R.L., and Vunjak-Novakovic, G. Development of silk-based scaffolds for tissue engineering of bone from human adipose-derived stem cells. Acta Biomater **8,** 2483, 2012.

13. Awada, H.A., Wickhama, M.Q., Leddya, H.A., Gimbleb, J.M., and Guilak, F. Chondrogenic differentiation of adipose-derived adult stem cells in agarose, alginate, and gelatin scaffolds. Biomaterials **25,** 3211, 2004.

14. Chung, S.Y., Krivorov, N.P., Rausei, V., Thomas, L., Frantzen, M., Landsittel, D., et al. Bladder reconstitution with bone marrow derived stem cells seeded on small intestinal submucosa improves morphological and molecular composition. J Urol **174,** 353, 2005.

15. Staack, A.H.S., Baskin, L.S., and Cunha, G.R. Molecular, cellular and developmental biology of urothelium as a basis of bladder regeneration. Differentiation **73,** 121, 2005.

16. Piechota, H.J., Gleason, C.A., Dahms, S.E., Dahiya, R., Nunes, L.S., Lue, T.F., et al. Bladder acellular matrix graft: in vivo functional properties of the regenerated rat bladder. Urol Res **27,** 206, 1999.

17. Obara, T., Matsuura, S., Narita, S., Satoh, S., Tsuchiya, N., and Habuchi, T. Bladder acellular matrix grafting regenerates urinary bladder in the spinal cord injury rat. Urology **68,** 892, 2006.

18. Pariente, J.L., Kim, B.S., and Atala, A. In vitro biocompatibility evaluation of naturally derived and synthetic biomaterials using normal human bladder smooth muscle cells. J Urol **167,** 1867, 2002.

19. Gilding, D.K. Biodegradable polymers. In: Williams, D.F., eds. Biocompatibility of Clinical Implant Materials. CRC Press, Boca Raton, FL, 1981, pp. 209–232.

20. Uematsu, K., Hattori, K., Ishimoto, Y., Yamauchi, J., Habata, T., Takakura, Y., et al. Cartilage regeneration using mesenchymal stem cells and a three-dimensional poly-lactic-glycolic acid (PLGA) scaffold. Biomaterials **26,** 4273, 2005.

21. Blackwood, K.A., McKean, R., Canton, I., Freeman, C.O., Franklin, K.L., Cole, D., *et al.* Development of biodegradable electrospun scaffolds for dermal replacement. Biomaterials **29,** 3091, 2008.

22. Kijeńska, E., Prabhakaran, M.P., Swieszkowski, W., Kurzydlowski, K.J., and Ramakrishna, S. Electrospun biocomposite P(LLA-CL)/collagen I/collagen III scaffolds for nerve tissue engineering. J Biomed Mater Res Part B **100B,** 1093, 2012.

23. Giuliani, A., Manescu, A., Larsson, E., Tromba, G., Luongo, G., Piattelli, A., Mangano, F., Iezzi, G. and Mangano, C. In vivo regenerative properties of coralline-derived (biocoral) scaffold grafts in human maxillary defects: demonstrative and comparative study with beta-tricalcium phosphate and biphasic calcium phosphate by synchrotron radiation X-Ray microtomography. Clin Implant Dent Relat Res, 2013. [Epub ahead of print]; DOI: 10.1111/cid.12039.

24. Gigante, A., Busilacchi, A., Lonzi, B., Cecconi, S., Manzotti, S., Renghini, C., Giuliani, A. and Mattioli-Belmonte, M. Purified collagen I oriented membrane for tendon repair: An *ex vivo* morphological study. J Orthop Res **31,** 738, 2013.

25. Giuliani, A., Frati, C., Rossini, A., Komlev, V.S., Lagrasta, C., Savi, M., Cavalli, S., Gaetano, C., Quaini, F., Manescu, A., and Rustichelli, F. High-resolution X-ray microtomography for three-dimensional imaging of cardiac progenitor cell homing in infarcted rat hearts. J Tissue Eng Regen Med **5,** e168, 2011.

26. Torrente, Y., Gavina, M., Belicchi, M., *et al.* High-resolution X-ray microtomography for three-dimensional visualition of human stem cell Muscle homing. Febs Lett **580,** 5759, 2006.

27. Farini, A., Villa, C., Manescu, A., Fiori, F., Giuliani, A., Razini, P., Sitzia, C., Del Fraro, G., Belicchi, M., Meregalli, M., Rustichelli, F., and Torrente, Y. Novel insight into stem cell trafficking in dystrophic muscles. Int J Nanomed **7,** 3059, 2012.

28. Arfelli, F., Assante, M., Bonvicini, V., Cantatore, G., Castelli, E., Palma, L.D., *et al.* Low-dose phase contrast X-ray medical imaging. Phys Med Biol **43,** 2845, 1998.

29. Bronnikov, A.V. Reconstruction formulas in phase-contrast tomography. Optics Commun **171,** 239, 1999.

30. Bronnikov, A.V. Theory of quantitative phase-contrast computed tomography, J Opt Soc Am **A19,** 472, 2002.

31. Groso, A., Abela, R., and Stampanoni, M. Implementation of a fast method for high resolution phase contrast tomography .Opt Express **14,** 8103, 2006.

32. Della Bella, S., Taddeo, A., Calabrò, M.L., Brambilla, L., Bellinvia, M., *et al.* Peripheral blood endothelial progenitors as potential reservoirs of Kaposi's Sarcoma-Associated Herpesvirus. PLoS One **3,** e1520, 2008.

33. Colombo, E., Calcaterra, F., Cappelletti, M., Mavilio, D., and Della Bella, S. Comparison of fibronectin and collagen in supporting the isolation and expansion of endothelial progenitor cells from human peripheral blood. PLoS ONE **6,** e66734, 2013.

34. Brambilla, L., Boneschi, V., Taglioni, M., and Ferrucci, S. Staging of classic Kaposi's sarcoma: a useful tool for therapeutic choices. Eur J Dermatol **13,** 83, 2003.

35. Della Bella, S., Taddeo, A., Colombo, E., Brambilla, L., Bellinvia, M., *et al.* Human herpesvirus-8 infection leads to expansion of the preimmune/natural effector B Cell compartment. PLoS One **5,** e15029, 2010.

36. Stampanoni, M., Groso, A., Isenegger, A., Mikuljan, G., Chen, Q., Bertrand, A., *et al.* Trends in synchrotron-based imaging–the SLS experience. Proc SPIE **6318,** 63180M-1, 2006.

37. De Witte, Y., Boone M., Vlassenbroeck, J., Dierick, M., Von L. Bronnikov-oioled correction for x-ray computed tomography. JOSA A, **4,** 890–894, 2009.

38. Ishaug-Riley, S.L., Okun, L.E., Prado, G., Applegate, M.A., and Ratcliffe, A. Human articular chondrocyte adhesion and proliferation on synthetic biodegradable polymer films. Biomaterials **20,** 2245, 1999.

39. Negroni, E., Riederer, I., Chaouch, S., Belicchi, M., Razini, P., Di Santo, J., Torrente, Y., Butler-Browne, G., and Mouly, V. *In vivo* Myogenic Potential of Human CD133 + Muscle-derived stem cells: a quantitative Study. Mol Ther **17,** 1771, 2009.

40. Bentzinger, C.F., Wang, Y.X., von Maltzahn, J., and Rudnicki, M.A. The emerging biology of muscle stem cells: implications for cell-based therapies. Bioessays **35,** 231, 2013.

41. Mesri, E.A., Cesarman, E., and Boshoff, C. Kaposi's sarcoma and its associated herpesvirus. Nat Rev **10,** 707, 2010.

42. Willians, D.F., and Mort, E. Enzyme-accelerated hydrolysis of polyglycolic acid. J Bioeng **1,** 231, 1977.

43. Li, S.M., Garreau, H., and Vert, M. Structure property relationship in the case of the degradation of massive poly(α-hydroxy acids) in aqueous media, Part 1: poly (DL-lactic acid). J Mater Sci Mater Res **1,** 123, 1990.

44. Causa, F., Netti, P.A., and Ambrosio, L. A multi-functional scaffold for tissue regeneration: the need to engineer a tissue analogue. Biomaterials **28,** 5093, 2007.

45. Hubbell, J.A. Biomaterials in tissue engineering. Biotechnology **13,** 565, 1995.

46. Place, E.S., Evans, N.D., and Stevens, M.M. Complexity in biomaterials for tissue engineering. Nat Mater **8,** 457, 2009.

47. Alberts, B., Johnson, A., Lewis, J., Raff, M., Roberts, K., and Walter, P. Molecular Biology of the Cell, 5th ed. Garland Science, New York, 2008.

48. Langer, R., and Vacanti, J.P. Tissue engineering. Science **260,** 920, 1993.

49. Davies, J.E., Causton, B., Bovell, Y., *et al.* The migration of osteoblasts over substrata of discrete surface charge. Biomaterials **7,** 231, 1986.

50. Dewez, J.-L., Lhoest, J.-B., Detrait, E., Berger, V., Dupont-Gillain, C.C., Vincent, L.-M., Schneider, Y.-J., Bertrand, P., and Rouxhet, P.G. Adhesion of mammalian cells topolymer surfaces: from physical chemistry of surfaces to selective adhesion of defined patterns. Biomaterials **19,** 1441, 1998.

51. Fiori, F., Giuliani, A., Manescu, A., Renghini, C., and Rustichelli, F. Synchrotron Radiation and Nanotechnology for Stem Cell Researchers. In Turksen, eds. Adult and Embryonic Stem Cells—Stem Cell Biology and Regenerative Medicine. ©Springer Science-Business Media, LLC, Philadelphia, PA 2012 pp. 81–102.

Address correspondence to:
Alessandra Giuliani, PhD
Dipartimento di Scienze Cliniche
Specialistiche e Odontostomatologiche
Università Politecnica delle Marche
Via Brecce Bianche 1
Ancona 60131
Italy

E-mail: a.giuliani@univpm.it